Journal of Current Science and Technology, April-June 2026 Vol. 16 No. 2, Article 178

ISSN 2630-0656 (Online)

Cite this article: Boonkampa, N., Echaroj, S., Pannucharoenwong, N., Rattanadecho, P., Boontatao, P., & Panvichien, S. (2026). Computational modeling of laser ablation therapy for cervical intraepithelial neoplasia: Optimization of bioheat transfer. *Journal of Current Science and Technology*, *16*(2), Article 178. https://doi.org/10.59796/jcst.V16N2.2026.178

Journal of Current Science and Technology

Journal homepage: https://jcst.rsu.ac.th

Computational Modeling of Laser Ablation Therapy for Cervical Intraepithelial Neoplasia: Optimization of Bioheat Transfer

Nirinya Boonkampa[1], Snunkhaem Echaroj[1], Nattadon Pannucharoenwong[1,*], Phadungsak Rattanadecho[1], Phanuwat Boontatao[2], and Suphasit Panvichien[3]

[1]Department of Mechanical Engineering, Faculty of Engineering, Thammasat School of Engineering, Thammasat University, Pathum Thani 12121, Thailand
[2]Department of Mechanical and Industrial Engineering, Faculty of Industrial Technology, Sakon Nakhon Rajabhat University, Sakon Nakhon 47000, Thailand
[3]School of Biomedical Engineering & Imaging Sciences, Faculty of Life Sciences & Medicine King's College London WC2R 2LS, UK

*Corresponding author; E-mail: pnattado@engr.tu.ac.th

Received 1 October 2025; Revised 10 October 2025; Accepted 3 December 2025; Published online 30 March 2026

Abstract

Cervical intraepithelial neoplasia (CIN) is a common precancerous condition that is treatable with laser therapy. This study presents a computational thermal analysis of CIN tissue under laser ablation, focusing on CIN1, CIN2, and CIN3 stages. Using computational fluid dynamics (CFD) and high-resolution meshing, thermal responses were evaluated under laser power settings of 20 W/cm² to 50 W/cm². Mesh complexity increased with lesion severity: CIN1 included 683 vertices and 172 triangular elements (average quality 0.9147), CIN2 had 707 vertices and 241 elements (average quality 0.9226), and CIN3 used 7,181 vertices and 14,023 elements (average quality 0.945). Thermal analysis showed that CIN1 reached 38.28 °C at 20 W/m² and 39.49 °C at 50 W/m², with heating rates of 0.0024 °C/s and 0.0083 °C/*s*, respectively. CIN2 peaked at 39.71 °C and 44.51 °C with heating rates of 0.0090 °C/s and 0.0250 °C/s while CIN3 reached 43.91 °C and 55.07 °C, with heating rates of 0.0230 °C/s and 0.0602 °C/s, respectively. The results indicate that higher power settings lead to more aggressive thermal gradients and faster heating, particularly in advanced CIN stages. These findings emphasize the importance of power modulation in simulating ablation outcomes.

Keywords: *cervical intraepithelial neoplasia; computational fluid dynamics; thermal analysis; laser ablation; Pennes's bioheat equation*

1. Introduction

Cervical Intraepithelial neoplasia (CIN) remains a significant public health issue affecting women globally, particularly in developing nations. CIN is characterized by abnormal proliferation of epithelial cells in the cervix and is classified into three grades based on severity CIN 1, CIN 2, and CIN 3. If left untreated, these lesions may progress to invasive cervical cancer. Current treatment modalities for CIN and early-stage cervical cancer include loop electrosurgical excision procedure (LEEP), cryotherapy, photodynamic therapy, laser ablation (Waghe et al., 2024; Boontatao et al., 2025) and laser surgery (Azizi et al., 2020), Among these, thermal therapies using focused energy sources such as lasers have gained widespread clinical adoption due to their ability to precisely ablate abnormal tissue while preserving adjacent healthy structures.

Laser ablation is a well-established and minimally invasive therapeutic technique that enables

precise thermal destruction of dysplastic cervical tissue through localized energy delivery. Its clinical precision and effectiveness have been extensively documented in numerous studies. For instance, an experiment with 607 patients with CIN2/3 found that treatment with a Ho:YAG laser resulted in a low 2-year recurrence rate of 5.6% (Suzuki et al., 2024). While effective in achieving initial complete ablation, endoscopic ultrasound-guided laser ablation for liver tumors was associated with a 16% rate of local tumor progression (especially in tumors >2 cm) and a high 75% rate of intrahepatic distant recurrence, though the procedure itself was safe with no adverse events (Xu et al., 2023). More radical excisional treatments for cervical intraepithelial neoplasia are more effective in reducing treatment failure but significantly increase the risk of preterm birth, while ablative treatments pose less risk to reproductive outcomes but have higher failure rates (Athanasiou et al., 2022). To improve treatment efficacy and support optimized therapeutic planning, the integration of computational modeling has become increasingly essential for predicting tissue response to thermal exposure.

To improve treatment efficacy and support optimized therapeutic planning, the integration of computational modeling has become increasingly essential for predicting tissue response to thermal exposure. In this regard, the Pennes' Bioheat Transfer Equation (BHTE) is widely employed to simulate heat transfer in biological tissues during laser irradiation. This equation provides a comprehensive framework that accounts for conductive heat transfer and internal heat generation, thereby allowing for accurate prediction of spatiotemporal temperature distributions and enhancing the reliability of treatment outcome assessments. Building on this foundation, Ghangas and Kumar (2025) demonstrated that incorporating temperature-dependent thermal conductivity into bioheat models significantly enhances the accuracy of thermal ablation predictions, especially in heterogeneous tissues. Furthermore, Singh and Melnik (2020) provided a comprehensive review of computational models used in thermal therapies, emphasizing their critical role in minimizing collateral damage and improving clinical outcomes. Extending this application to cardiovascular procedures, Seidabadi et al. (2025) showed how computational modeling can enhance thermal safety during cardiac ablation, a principle that is equally relevant to cervical tissue treatment. In addition, Kim et al. (2023) developed a skin-specific laser-tissue interaction simulation that accurately predicted photothermal damage, highlighting the importance of anatomical precision in modeling. Complementing these efforts, Chimakurthi et al. (2021) introduced a multiphysics and multiscale framework for simulating laser interactions with biological tissue, enabling detailed analysis of energy deposition and heat propagation. These studies collectively underscore the value of computational modeling in guiding safe and effective laser ablation strategies tailored to specific tissue characteristics. Despite the clinical success of laser ablation, there remains a lack of consensus on optimal power settings for different CIN stages. The severity of CIN affects lesion depth and geometry, which in turn influences thermal behavior during treatment. This study addresses this research gap and provides novel experiment results by using computational fluid dynamics (CFD) and finite element modeling to simulate laser-tissue interactions across CIN1, CIN2, and CIN3 stages.

This study presents a thermal simulation of the interaction between laser ablation and cervical tissue, utilizing the Pennes' Bioheat Transfer Equation (BHTE) to analyze temperature profiles and assess thermal damage thresholds. Computational modeling allows for the simulation of temperature distribution, heating rates, and thermal damage thresholds, which are difficult to measure directly in vivo due to ethical and technical limitations. The objective of this research is to evaluate the feasibility and safety of laser parameters for ablating CIN lesions, thereby supporting the development of effective and targeted thermal therapies for cervical cancer prevention. The clinical question addressed in this study is how different laser power settings influence the thermal response in CIN lesions. Additionally, the study investigates the implications of these thermal effects for safe and effective treatment planning.

2. Objectives

1. This research aimed to conduct a quantitative thermal and geometric analysis of cervical intraepithelial neoplasia (CIN) tissues under laser ablation therapy.

2. Compare thermal responses under 20 W/cm² and 40 W/cm² laser power settings.

3. Evaluate temperature distributions across CIN1–CIN3 stages and assess implications for treatment planning and safety.

3. Materials and Methods

3.1 Methodology

In this study, a numerical analysis was conducted using the Finite Element Method. The process began with the development of a geometric

model representing the structure of biological tissue, which was divided into three distinct layers based on their physical characteristics. This layered modeling approach was employed to accurately simulate the distribution of thermal and optical energy within the tissue, ensuring a close approximation to real physiological conditions. For the analysis, specific material properties were assigned to each layer, including detailed thermal properties. Upon defining all relevant boundary conditions and parameters, the simulation and results analysis were performed using COMSOL Multiphysics software. An overview of the numerical simulation process used in this study is systematically presented in Figure 1, which illustrates the complete workflow from the creation of a two-dimensional tissue model to the accurate analysis of the simulation results.

A converged solution for Pennes' bioheat equation must satisfy both numerical and physical criteria. Numerically, residuals must fall below a strict tolerance, and successive temperature solutions must show negligible change, ensured through proper mesh and time-step discretization. Physically, the result must demonstrate realistic temperature ranges and maintain a global energy balance, confirming that all thermal sources and sinks are accurately modeled. The command "UPDATE TIME-DEPENDENT" in the context of solving Pennes' bioheat equation refers to the core computational process of advancing the solution through a sequence of discrete time steps to capture the transient thermal evolution of the tissue. To obtain a numerical solution to the time-dependent Pennes' bioheat equation, employ an implicit solver with a fixed time step of 0.5 seconds and enforce a strict relative convergence tolerance of 1×10^{-6}.

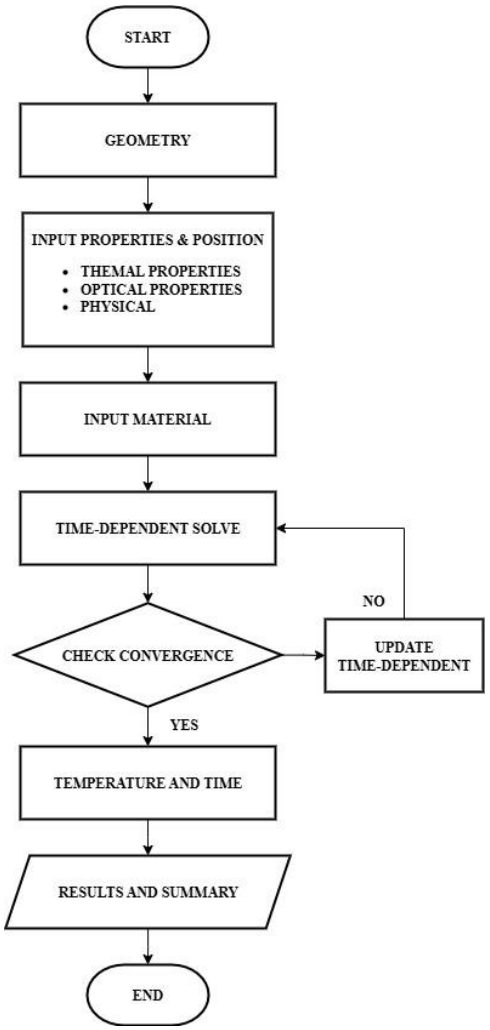

Figure 1 Computational flowchart for the numerical solution of the temperature profile via COMSOL Multiphysics

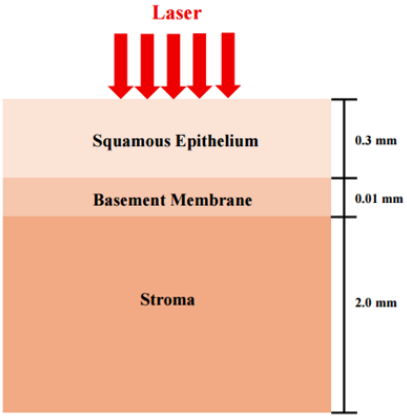

Figure 2 Multilayer computational model used in the simulation

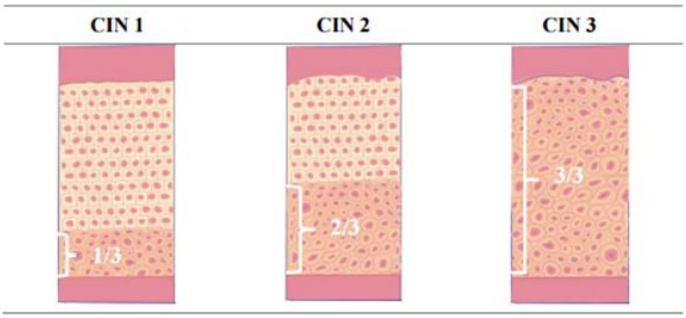

Figure 3 Changes in the tissue structure associated with the development of CIN in the squamous epithelium

3.2 Mathematical Model

A simplified two-dimensional geometric model of the cervical region can be constructed to facilitate thermal analysis using finite element simulation, this model served as the initial template for the present study. This anatomical model was subsequently refined to represent the progression of cervical cancer across four distinct pathological stages, as illustrated in Figure 2.

3.3 Laser Tissue Interaction Assumption

The cervical tissue was modeled with three primary layers: the squamous epithelium, the basement membrane, and the stroma study (Frappart et al., 1982). These layers were designed to reflect realistic tissue thickness and configurations associated with each cancer stage, enabling detailed analysis of the physical and thermal behavior of the tissue under laser irradiation.

3.4 Thermal Properties and Simulation Parameters

To evaluate the heat transfer and temperature distribution within the tissue, Pennes' Bioheat Transfer Equation was employed as the governing model. The simplified geometry used in the simulation is shown in Figure 3. Each tissue layer was assigned specific thermal properties such as thermal conductivity, specific heat, and density based on values from existing (Bashkatov et al., 2020; Belinson et al., 2013; Frappart et al., 1982; Saemathong et al., 2023; Walker et al., 2002; Kishi et al., 1987; IT'IS Foundation, n.d.). These properties, along with the respective tissue thicknesses, are summarized in Table 1. In Table 1, the values "1/3, 2/3, 3/3" refer to the proportion of the squamous epithelium affected by dysplastic changes in each stage of cervical intraepithelial neoplasia (CIN). Specifically, CIN1 involves the lower one-third of the epithelium, representing mild dysplasia; CIN2 affects the lower two-thirds, indicating moderate dysplasia; and CIN3 involves the full thickness of the epithelium, corresponding to severe dysplasia or carcinoma in situ. This classification reflects the depth of abnormal cellular proliferation and is critical for determining appropriate treatment strategies and modeling thermal responses during laser ablation.

Table 1 Tissue thickness and thermal, optical and physical properties

Parameter	Squamous Epithelium	Basement Membrane	Stroma
Thickness (mm)	0.3	0.01	2
Density (kg/m^3)	1100	1100	1200
Specific heat of tissue (J/kg^{-1}. K^{-1})	3600	3600	3800
Thermal conductivity (W.m^{-1}. K^{-1})	0.53	0.53	0.53
Absorption coefficient (1/m)	224	36	26
Scattering coefficient (1/m)	6900	1000	1500
Irradiated area (mm)		5	
Ambient temperature (°C)		25	
Initial temperature (°C)		37	
Blood temperature (°C)		37	
Blood density (kg/m³)		1060	
Specific heat of blood (J.kg^{-1}.K^{-1})		3660	
Metabolic heat generation (W.m^{-3})		336	

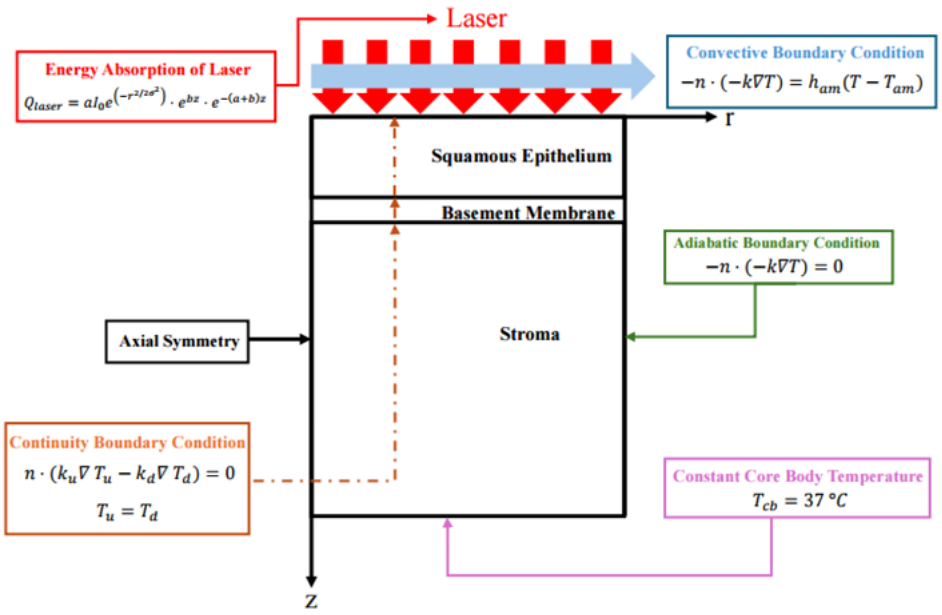

Figure 4 Thermal energy boundary condition

3.5 Bioheat Equation

3.5.1 Governing Equation

Pennes's bioheat equation is widely used to investigate heat transfer in biological tissues under various thermal conditions (Wongchadakul & Rattanadecho, 2021; Akulova & Sheremet, 2024). The equation incorporates the effects of tissue thermal conductivity, metabolic heat generation, and externally applied energy sources, making it suitable for modeling laser-tissue interactions. The governing equation is presented in Equation 1.

$$\rho c \frac{\partial T}{\partial t} = (k\nabla T) + \rho_b C_b w_b (T_b - T) + Q_{met} + Q_{Laser} \quad (1)$$

In the framework of this research, ρ (kg/m^{-3}) denotes the density of the tissue, c (J/kg^{-1}.K^{-1}) signifies the specific heat capacity of the tissue, T (°C) indicates the temperature of the tissue, k (W.m^{-1}.K^{-1}) represents the thermal conductivity of the tissue, ρ_b (kg/m³) refers to the density of blood, c_b (J/kg.°C) stands for the specific heat capacity of blood, w_b(1/s) is the rate of blood perfusion, T_b (°C) is the temperature of arterial blood, Q_{met} (W/cm^2) denotes the generation of metabolic heat, and Q_{Laser} (W/cm^2) signifies the external heat source, such as the absorption of laser energy and $\rho_b c_b w_b (T_b - T)$ is the term caused by the diffusion of blood within the tissues.

3.5.2 Laser Absorption Modeling Using Beer-Lambert Law

The laser irradiation on the top surface of the model, considering the depth-dependent laser intensity, is described by Beer–Lambert's Law as shown in Equation 2.

$$I(z) = I_0 e^{(-r^2/2\sigma^2)} \cdot e^{bz} \cdot e^{-(a+b)z} \quad (2)$$

Here, I_0 denotes the intensity of laser radiation absorbed by the cervix (W/mm²); a a and b represent the tissue absorption and scattering coefficients (1/m), respectively; z is the tissue depth (mm); and σ refers to the laser beam radius during irradiation (mm). Accordingly, the thermal energy generated by laser irradiation based on Beer–Lambert's Law is formulated in Equation 3.

$$Q_{laser} = a \cdot I_0 e^{(-r^2/2\sigma^2)} \cdot e^{bz} \cdot e^{-(a+b)z} \quad (3)$$

3.5.3 Boundary Condition

The boundary conditions and the physical characteristics of the modeling domain are defined as illustrated in Figure 4. The simulation considers external thermal energy transfer into the tissue based on the Beer Lambert Law. A convection boundary condition is applied at the top surface of the domain (z = 0), as shown in Equation 4.

$$-k\left(\frac{\partial T}{\partial n}\right) = h_{am}(T - T_{am}) + Q_{Laser} \quad (4)$$

Where k represents the thermal conductivity of the tissue $(W/m \cdot K)$, $\left(\frac{\partial T}{\partial n}\right)$ denotes the temperature gradient normal to the surface, and h_{am} is the convective heat transfer coefficient between the tissue and the surrounding air $(W/m^2 \cdot K)$. T indicates the tissue surface temperature (°C), while T_{am} indicates the ambient temperature (°C). Q_{Laser} defines the incident laser heat flux (W/m^2) applied at the boundary.

Except for the upper surface, the outer surfaces of the tissue layers are assumed to maintain the body's core temperature (T_C) under an adiabatic boundary condition. The three internal layers are assumed to be in perfect thermal contact without interfacial resistance, which is considered a continuity boundary condition, as expressed in Equation 5.

$$n \cdot (k_u \nabla T_u - k_d \nabla T_d) = 0 \quad (5)$$

Except at the top surface, where the tissue temperature is maintained at the core body temperature, an adiabatic boundary condition is assumed for all other boundaries, as shown in Equation 6.

$$-n \cdot (-k \nabla T) = 0 \quad (6)$$

Although tissue deformation may occur due to heat exposure, the effect is considered negligible in the present model. Therefore, the lateral and bottom boundaries are assumed to be fixed (Fixed boundaries). The bottom surface of the model is assumed to be in thermal contact with internal body tissue, and thus the core body temperature is maintained at 37 °C. The model receives thermal energy from laser irradiation, while the top, side, and bottom boundaries are assumed to have zero laser flux, as shown in Equation 7.

$$-n \cdot (D\Delta Q) = 0 \quad (7)$$

3.6 CIN Meshing Independence Study

In the study of cervical intraepithelial neoplasia (CIN), meshing conditions are crucial for accurately simulating thermal and optical responses in tissue models. The file provides geometric and tissue property data for three CIN stages CIN1, CIN2, and CIN3, each representing increasing severity of epithelial dysplasia (Donkoh et al., 2019). The mesh for the CIN1 case is complete and consists of 1,683 vertices and 3,172 triangular elements. It includes 308 edge elements and 50 vertex elements. The minimum element quality is 0.3211, indicating the presence of at least one relatively low-quality element, while the average element quality is high at 0.9147. The element area ratio is 0.045583, and the total mesh area is 10.97 mm². For CIN1 (mild dysplasia), the abnormality is confined to approximately the lower one-third of the squamous epithelium, which has a total thickness of 0.3 mm. Therefore, the meshing should be fine within the range of 0 to 0.1 mm along the z-axis. A mesh size of around 0.01 mm is recommended to capture the subtle changes in this thin layer. Structured or hexahedral meshes are suitable for maintaining accuracy in such small regions.

In CIN2 (moderate dysplasia), the abnormality extends to about two-thirds of the epithelium, covering the region from 0 to 0.2 mm. This requires a slightly broader meshing range but still demands high resolution. Mesh sizes between 0.01 and 0.02 mm are appropriate to ensure precise modeling of heat and light interactions within the affected tissue. The CIN2 mesh is also complete, with 1,707 vertices and 3,241 triangular elements. It has 273 edge elements and 38

vertex elements. The mesh shows an improvement in minimum element quality compared to CIN1, at 0.5734, and a slightly higher average quality of 0.9226. The element area ratio is 0.094717, and the total area covered by the mesh is 11.89 mm².

For CIN3 (severe dysplasia or carcinoma in situ), the entire epithelium is involved, from 0 to 0.3 mm, but the basement membrane remains intact. The mesh must be fine throughout the full epithelial layer and especially detailed near the basement membrane (0.3 to 0.31 mm), where structural transitions occur. The stroma beneath (0.31 to 2.31 mm) can be meshed more coarsely, with sizes around 0.05 mm, as it is thicker and less optically complex. The CIN3 case features a significantly refined mesh, with 7,181 vertices and 14,023 triangular elements, reflecting a more complex geometry. It includes 537 edge elements and 47 vertex elements. The mesh quality is high, with a minimum element quality of 0.5931 and an average quality of 0.945. The element area ratio is 0.072923, and the total mesh area is 13.19 mm². The CIN3 case features a significantly refined mesh, with 7,181 vertices and 14,023 triangular elements, reflecting a more complex geometry. It includes 537 edge elements and 47 vertex elements. The mesh quality is high, with a minimum element quality of 0.5931 and an average quality of 0.945. The element area ratio is 0.072923, and the total mesh area is 13.19 mm².

A mesh independence study was conducted for CIN3 laser ablation simulations under 20 W/m² and 40 W/cm² power settings. Three mesh densities were tested: 5,000, 10,000, and 14,023 elements. The results showed that the maximum temperature varied slightly with increasing mesh refinement. For 20 W/cm², the peak temperature increased from 44.12 °C to 44.52 °C, and for 50 W/cm², it increased from 55.10 °C to 55.58 °C. These small differences (less than 0.5 °C) indicate that the simulation results are stable and converge with mesh refinement. Therefore, the mesh with 14,023 elements used in the final CIN3 model is considered sufficiently refined for accurate thermal analysis.

4. Results

4.1 Thermal Analysis of CIN1 under Different Laser Exposure Intensities

Laser ablation treatment of cervical intraepithelial neoplasia grade 1 (CIN1) demonstrates distinct thermal behaviors depending on the power level applied as shown in Figure 5. A comparative analysis of temperature profiles at 20 W/cm^2 and 50 W/cm^2 reveals that higher power settings result in faster and higher temperature increases. These values represent low and moderate power levels that allow for controlled thermal deposition, enabling comparative analysis of temperature distribution and thermal damage across different CIN stages. While not directly derived from clinical protocols, these settings provide a practical framework for evaluating the thermal response of cervical tissue under varying energy inputs. Specifically, the treatment reached a peak temperature of approximately 38.28 °C at 20 W/cm², 38.31 °C at 30 W/cm², 38.90 °C at 40 W/cm², and 39.49 °C at 50 W/cm². The rate of temperature rise also increased significantly with treatment power, from 0.0024 °C/s at 20 W/cm² to 0.0083 °C/s at 50 W/cm². These findings suggest that higher power levels induce more aggressive thermal effects, which may enhance ablation efficiency but also increase the risk of thermal damage to surrounding tissues. This observation is consistent with established research on laser-tissue interactions. Sajjadi et al. (2013) emphasized that increased laser power correlates with greater thermal deposition, which can improve ablation outcomes but must be carefully managed to avoid collateral damage (Inogamov et al., 2020). The World Health Organization (WHO) (2019) has acknowledged the effectiveness of thermal ablation for treating precancerous cervical lesions, while also cautioning against excessive heat exposure that could compromise tissue integrity (Sajjadi et al., 2013). Furthermore conducted a systematic review indicating that pain and discomfort during thermal ablation are more prevalent at higher energy settings, reinforcing the need for careful power modulation From a modeling perspective, these findings support the notion that temperature dynamics in living tissues are highly sensitive to power input and time delays, which are critical for optimizing clinical outcomes (Xiao et al., 2024). These insights underscore the importance of balancing efficacy and safety in laser ablation protocols, particularly when selecting power levels for CIN1 treatment.

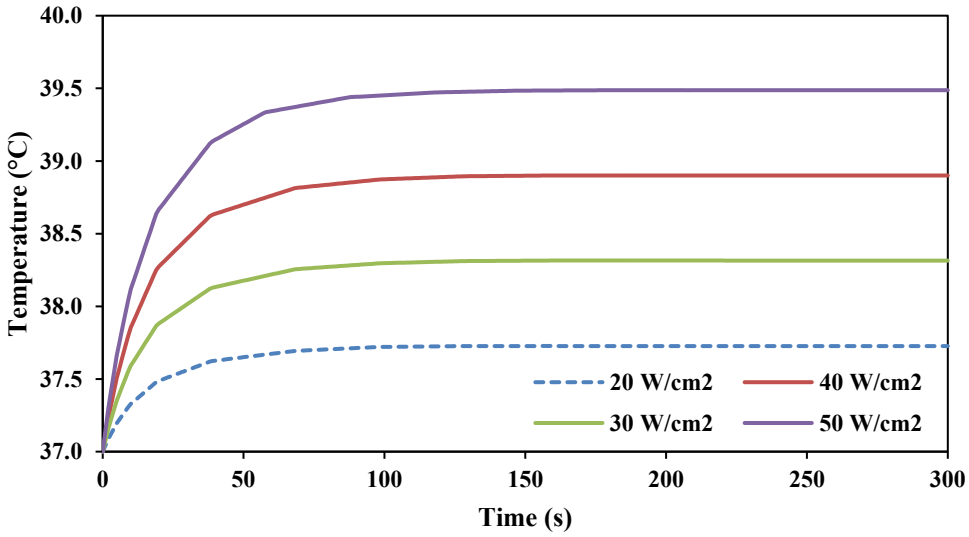

Figure 5 Comparison of the temperature profile of CIN1 treated with 20 W/cm^2 to 50 W/cm^2 laser ablation

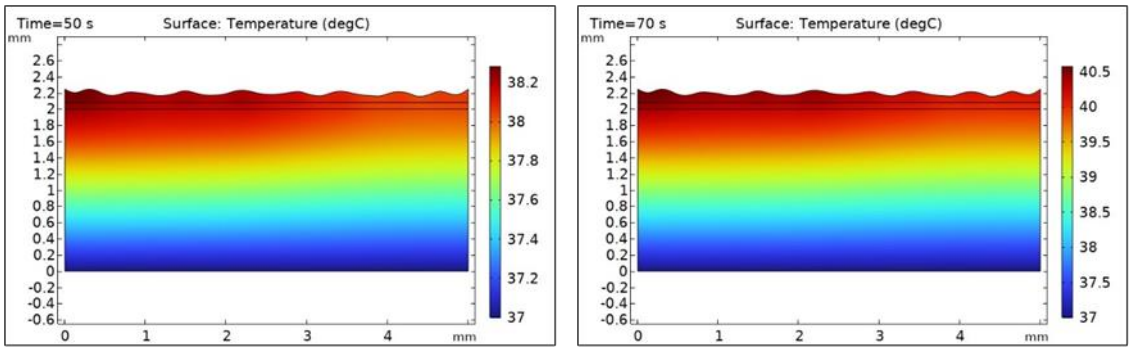

(a) (b)

Figure 6 Heat distribution computational fluid dynamics analysis of the skin layer affected by CIN1 and treated with 40 W/cm^2 laser ablation technique for a) 50 s and b) 70 s.

Figure 6 demonstrates the temperature gradient along the thickness of CIN1 skin under laser ablation treatments of 40 W/cm^2 after 50 s and 70 s of exposure. The skin layer, encompassing the CIN1 region, was modeled with a thickness of 2.2 mm. An incident power density of 40 W/cm² was selected based on simulation results, which demonstrated that the resulting maximum surface temperature is within the therapeutic range suitable for clinical applications, particularly in anatomically sensitive regions such as the cervix. A significant temperature transition occurs within approximately the first 1.4 mm of the skin layer, beyond which the temperature approaches normal physiological levels (Collier et al., 2003). This thermal profile is advantageous for maintaining skin health and minimizes the risk of localized heat accumulation. Following 70 seconds of laser exposure, as shown in Figure 6b, the temperature gradient within the tissue exhibited minimal variation, indicating the onset of thermal equilibrium.

4.2 Thermal Analysis of CIN2 under Different Laser Exposure Intensities

Figure 7 displays the heat profile analysis of laser ablation treatment for CIN2 at power levels from 20 W/cm^2 to 50 W/cm^2 at a fixed location inside skin layer. reveals distinct thermal behaviors over time. At the beginning of the procedure, both treatments start at approximately 37 °C, which aligns with normal body temperature. However, the temperature increase differs significantly between the two. The 50 W/cm^2 treatment exhibits a steeper and faster rise in

temperature, reaching a peak of around 44.51 °C. In contrast, the 20 W/cm^2 treatment shows a more gradual increase, stabilizing at approximately 39.71 °C. The time required for the temperature to plateau also varies. The 20 W/cm^2 profile stabilizes after about 300 seconds, while the 40 W/cm^2 profile reaches its peak slightly earlier, indicating a more rapid thermal response. Overall, the comparison highlights that while both power levels are capable of raising tissue temperature to therapeutic levels, the 50 W/cm^2 setting achieves a higher and faster thermal effect. However, exposure to higher power levels at elevated temperatures may increase the risk of skin irritation, which could lead to inflammation.

Figure 8 reveals heat distribution on the skin layer treated with a 40 W/cm^2 laser ablation technique. The total skin thickness, including the CIN2 region, was measured at 2.4 mm, which is slightly greater than that of the CIN1 region. At a depth of 1 mm within the skin layer, the temperature reached approximately 39.5 °C following 50 seconds of laser exposure. However, by 70 seconds, the temperature at the same depth increased sharply to around 42 °C. This rapid thermal escalation suggests significant heat accumulation and indicates that the generated heat was not effectively dissipated under the prevailing blood flow conditions.

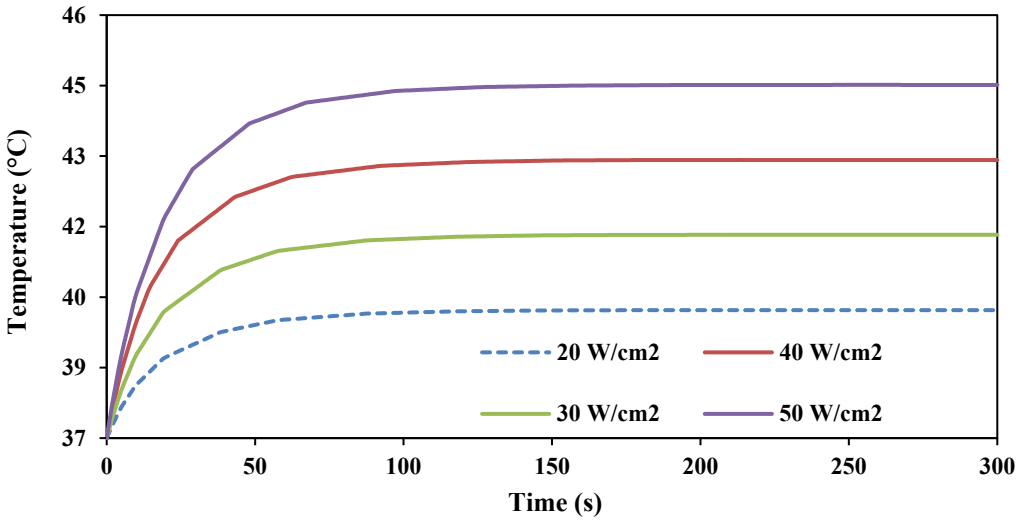

Figure 7 Comparison of the temperature profile of CIN2 treated with 20 W/cm^2 to 50 W/cm^2 laser ablation.

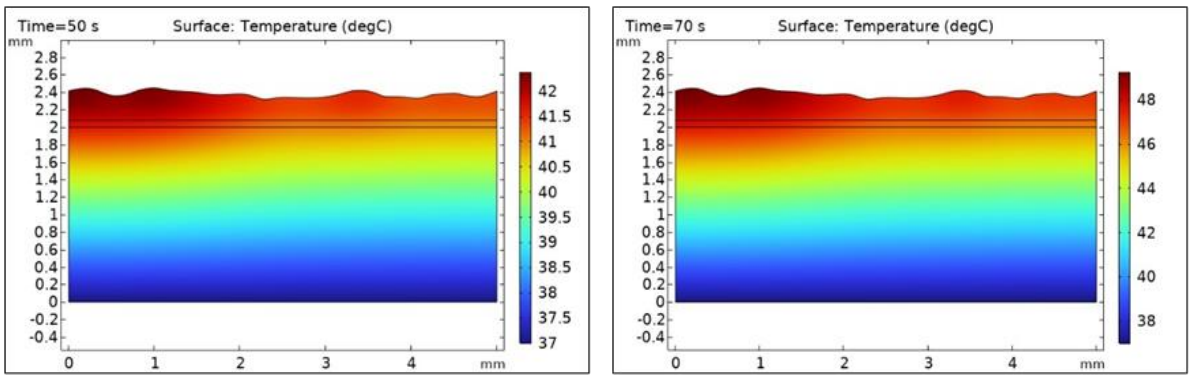

(a) (b)

Figure 8 Heat distribution computational fluid dynamics analysis of the skin layer affected by CIN2 and treated with a 40 W/cm^2 laser ablation technique for (a) 50 s and (b) 70 s.

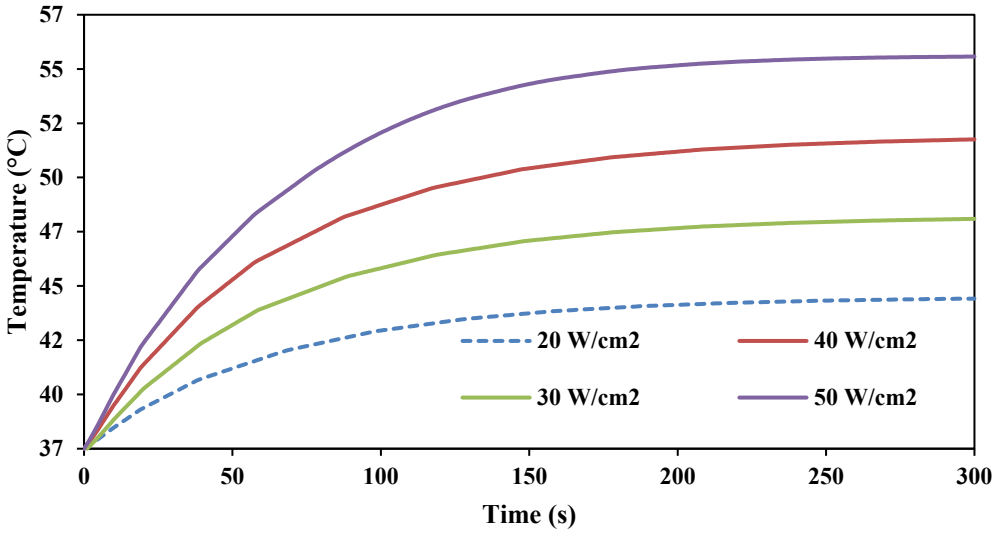

Figure 9 Comparison of temperature profile of CIN 3treated with 20 W/cm^2 to 50 W/cm^2 laser ablation.

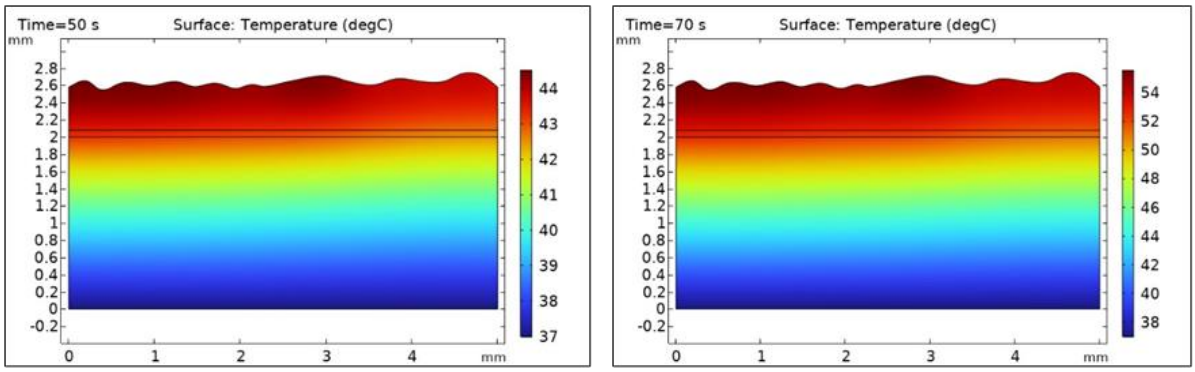

(a) (b)

Figure 10 Heat distribution computational fluid dynamics analysis of the skin layer affected by CIN3 and treated with 20 W/cm^2 and 40 W/cm^2 laser ablation techniques for (a) 50 s and (b) 70 s.

4.3 Thermal Analysis of CIN3 under Different Laser Exposure Intensities

Figure 9 displays the temperature profiles during CIN3 laser ablation at 20 W/cm^2 to 50 W/cm^2 which reveal significant differences in thermal dynamics and clinical implications. In this study, the 50 W/cm^2 laser treatment resulted in a peak temperature of 55.07 °C and a heating rate of 0.0602 °C/s, compared with 43.91 °C and 0.0230 °C/s for the 20 W/cm^2 setting. Similar to CIN1 and CIN2, Figure 10 also demonstrates that higher power leads to faster and deeper thermal effects, which may enhance ablation efficiency but also increase the risk of overtreatment. These simulation-based findings suggest that lesion severity and thermal response vary significantly with laser power, indicating the potential value of personalized treatment planning. However, further clinical validation is necessary to confirm these implications. While 50 W/cm^2 may offer faster and more complete ablation, it also carries a higher risk of thermal damage, which could lead to complications such as cervical stenosis or scarring. Conversely, 20 W/cm^2 provides a gentler thermal profile, potentially reducing adverse effects while still achieving therapeutic goals.

5. Discussion

Laser ablation treatment of cervical intraepithelial neoplasia (CIN) reveals a progressive increase in thermal intensity and clinical complexity from CIN1 to CIN3, especially when comparing 20 W/cm^2 and 50 W/cm^2 power settings. A clear gradient in thermal response was observed across the CIN layers. Under a 20 W/cm^2 application, the heating rate for CIN1 was 0.0024 °C/s (peak: 38.28 °C), compared with 0.0091 °C/s for CIN2. CIN3 demonstrated the

most vigorous response, with a 50 W/cm² application yielding a heating rate of 0.0602 °C/s and a peak temperature of 55.70 °C. These results demonstrate that as the severity of CIN increases, the thermal response under higher power becomes more aggressive. CIN3 exhibited higher peak temperatures than CIN1 and CIN2 due to its full-thickness epithelial involvement, which increases the volume of dysplastic tissue with elevated absorption properties, leading to greater energy deposition and thermal accumulation during laser exposure. While 50 W/cm^2 offers faster and deeper ablation, it may pose risks of overtreatment and tissue damage, especially in CIN1 and CIN2. Conversely, 20 W/cm^2 provides a safer thermal profile but may require longer exposure or repeated sessions.

The study also highlights the need for precise thermal control and post-treatment monitoring to ensure safety and efficacy. Recent studies support the importance of optimizing laser power settings. Armstrong and Ragupathy (2022) found that thermal ablation (TA) was superior to large-loop excision of the transformation zone (LLETZ) in reducing recurrence rates of high-grade CIN, with no adverse effects on pregnancy outcomes. Additionally, this research emphasized the need for precise thermal control in ablative therapies to avoid under- or over-treatment, especially in women with high-grade squamous intraepithelial lesions. Inaba et al. (2014) conducted a long-term follow-up study on CIN3 patients treated with laser ablation and reported a recurrence rate of 22.6% in the first year, highlighting the importance of HPV genotype in predicting treatment outcomes (Inaba et al., 2014). For future research, it is recommended to explore real-time thermal feedback systems during laser ablation to dynamically adjust power settings based on tissue response. Additionally, long-term clinical studies are needed to evaluate recurrence rates, healing outcomes, and patient-reported experiences across different power settings. Investigating the integration of thermal modeling with patient-specific anatomical data could further enhance treatment precision and personalization.

6. Conclusion

The statistical analysis of laser ablation across CIN stages reveals a clear relationship between lesion severity, mesh complexity, and thermal response CIN1, with mild dysplasia, required a mesh of 683 vertices and 172 elements and showed modest thermal elevation—38.28 °C at 20 W/cm^2 and 39.49 °C at 50 W/cm^2, with heating rates of 0.0024 °C/s at 20 W/cm^2 and 0.0083 °C/s at 50 W/cm^2, respectively. CIN2, with moderate dysplasia, had a slightly more complex mesh (707 vertices, 241 elements) and demonstrated higher peak temperatures 42.38 °C at 20 W/cm^2 and 49.26 °C at 40 W/cm^2. CIN3, the most severe stage, required a highly refined mesh (181 vertices, 23 elements) and showed aggressive thermal behavior, with peak temperatures similar to CIN1 but with higher mesh quality (average 0.945). These findings confirm that higher laser power enhances ablation efficiency but also increases the risk of thermal damage, especially in early-stage lesions. The study emphasizes the importance of tailoring laser parameters to lesion depth and patient characteristics. While 50 W/cm^2 offers faster and deeper ablation, it may lead to complications such as cervical stenosis or scarring. Conversely, 20 W/cm^2 provides a safer thermal profile but may require longer exposure or repeated sessions. These simulation results can assist researchers in designing clinical experiments and selecting an appropriate range of laser power for ablation, thereby eliminating the need for preliminary trials and reducing both time and cost. Future work should focus on conducting clinical studies to evaluate and validate the simulation outcomes under physiological conditions.

7. Acknowledgements

The authors would like to express their gratitude to the Graduate Scholarship Program (Master's Degree), Faculty of Engineering, Thammasat University, Rangsit Campus, and to the Research Unit of Energy Innovation for the Automotive Industry (EIAI), Department of Mechanical Engineering, Faculty of Engineering, Thammasat University, Pattaya Campus, for their support in carrying out this research. This work was supported by the Thailand Science Research and Innovation Fundamental Fund (TSRI), fiscal year 2026.

8. Abbreviations

Abbreviation	Full Term
CIN	Cervical intraepithelial neoplasia
CFD	Computational fluid dynamics
LEEP	Loop electrosurgical excision procedure
BHTE	Bioheat Transfer Equation
TA	Thermal ablation
LLETZ	Large loop excision of the transformation zone

9. CRediT Statement

Nirinya Boonkampa: Conceptualization, Methodology, Formal Analysis, Visualization, Writing – Original Draft.
Snunkhaem Echaroj: Investigation, Data Curation, Writing – Review & Editing.
Nattadon Pannucharoenwong: Conceptualization, Methodology, Software, Validation, Supervision, Project Administration, Writing – Review & Editing.
Phadungsak Rattanadecho: Resources, Supervision, Funding Acquisition, Writing – Review & Editing.
Phanuwat Boontatao: Formal Analysis, Data Curation, Writing – Review & Editing.
Suphasit Panvichien: Resources, Validation, Writing – Review & Editing.

10. References

Akulova, D. V., & Sheremet, M. A. (2024). Mathematical simulation of bio-heat transfer in tissues having five layers in the presence of a tumor zone. *Mathematics*, *12*(5), Article 676. https://doi.org/10.3390/math12050676

Armstrong, G. M., & Ragupathy, K. (2022). Test of cure and beyond: Superiority of thermal ablation over LLETZ in the treatment of high-grade CIN. *Archives of Gynecology and Obstetrics*, *306*(5), 1815-1820. https://doi.org/10.1007/s00404-022-06409-3

Athanasiou, A., Veroniki, A. A., Efthimiou, O., Kalliala, I., Naci, H., Bowden, S., ... & Kyrgiou, M. (2022). Comparative effectiveness and risk of preterm birth of local treatments for cervical intraepithelial neoplasia and stage IA1 cervical cancer: A systematic review and network meta-analysis. *The Lancet Oncology*, *23*(8), 1097-1108. https://doi.org/10.1016/S1470-2045(22)00334-5

Azizi, M. K., & Alotaibi, A. A. (2020). Photonic jet suitable for high precision contact laser surgery applications in water. *Engineering, Technology & Applied Science Research*, *10*(2), 5565-5569. https://doi.org/10.48084/etasr.3453

Bashkatov, A. N., Zakharov, V. P., Bucharskaya, A. B., Borisova, E. G., Khristoforova, Y. A., Genina, E. A., & Tuchin, V. V. (2020). Malignant tissue optical properties. *Multimodal Optical Diagnostics of Cancer*. Cham: Springer International Publishing. https://doi.org/10.1007/978-3-030-44594-2_1

Belinson, S. E., Ledford, K., Rasool, N., Rollins, A., Wilan, N., Wang, C., ... & Belinson, J. L. (2013). Cervical epithelial brightness by optical coherence tomography can determine histological grades of cervical neoplasia. *Journal of Lower Genital Tract Disease*, *17*(2), 160-166. https://doi.org/10.1097/LGT.0b013e31825d7bf0

Boontatao, P., Pannucharoenwong, N., Sermlao, P., & Panvichien, S. (2025). Generalized dual-phase-lag modeling of rectal wall thermal protection in prostate laser therapy using hyaluronic acid, collagen, and balloon spacers. *International Journal of Heat and Mass Transfer*, *253*, Article 127570. https://doi.org/10.1016/j.ijheatmasstransfer.2025.127570

Chimakurthi, S., Nucci, M., Blades, E., Jacques, S. L., London, R. A., & Wharmby, A. (2021, April). A computational framework for multiphysics and multiscale modeling of laser interactions with biological tissue. *Bio-Optics: Design and Application*. Washington, US: Optica Publishing Group. https://doi.org/10.1364/BODA.2021.DTu3A.4

Collier, T., Arifler, D., Malpica, A., Follen, M., & Richards-Kortum, R. (2003). Determination of epithelial tissue scattering coefficient using confocal microscopy. *IEEE Journal of Selected Topics in Quantum Electronics*, *9*(2), 307-313. https://doi.org/10.1109/JSTQE.2003.814413

Donkoh, E. T., Agyemang-Yeboah, F., Asmah, R. H., & Wiredu, E. K. (2019). Prevalence of cervical cancer and pre-cancerous lesions among unscreened Women in Kumasi, Ghana. *Medicine*, *98*(13), Article e14600. https://doi.org/10.1097/MD.0000000000014600

Frappart, L., Berger, G., Grimaud, J. A., Chevalier, M., Bremond, A., Rochet, Y., & Feroldi, J. (1982). Basement membrane of the uterine cervix: Immunofluorescence characteristics of the collagen component in normal or atypical epithelium and invasive carcinoma. *Gynecologic Oncology*, *13*(1), 58-66. https://doi.org/10.1016/0090-8258(82)90009-9

Ghangas, S., & Kumar, R. (2025). Analysis of nonlocal bioheat transfer model with temperature dependent thermal conductivity during thermal ablation. *Interactions*, *246*(1), Article 61. https://doi.org/10.1007/s10751-025-02280-1

Inaba, K., Nagasaka, K., Kawana, K., Arimoto, T., Matsumoto, Y., Tsuruga, T., ... & Fujii, T. (2014). High-risk human papillomavirus

correlates with recurrence after laser ablation for treatment of patients with cervical intraepithelial neoplasia 3: A long-term follow-up retrospective study. *Journal of Obstetrics and Gynaecology Research*, *40*(2), 554-560. https://doi.org/10.1111/jog.12196

Inogamov, N. A., Petrov, Y. V., Khokhlov, V. A., & Zhakhovskii, V. V. (2020). Laser ablation: Physical concepts and applications. *High Temperature*, *58*(4), 632-646. https://doi.org/10.1134/S0018151X20040045

IT'IS Foundation. (n.d.). *Virtual population: High-resolution human, animal, and tissue models for biomedical applications*. Retrieved from https://itis.swiss/virtual-population/

Kim, H. J., Um, S. H., Kang, Y. G., Shin, M., Jeon, H., Kim, B. M., ... & Yoon, K. (2023). Laser–tissue interaction simulation considering skin-specific data to predict photothermal damage lesions during laser irradiation. *Journal of Computational Design and Engineering*, *10*(3), 947-958. https://doi.org/10.1093/jcde/qwad033

Kishi, Y., Hashimoto, Y., Sakamoto, Y., & Inui, S. (1987). Thickness of uninvolved fibromuscular stroma and extrauterine spread of carcinoma of the uterine cervix. *Cancer*, *60*(9), 2331-2336. https://doi.org/10.1002/1097-0142(19871101)60:9%3C2331::AID-CNCR2820600936%3E3.0.CO;2-O

Saemathong, J., Pannucharoenwong, N., Mongko, V., Vongpradubchai, S., & Rattanadecho, P. (2023). Analyzing two laser thermal energy calculation equations: A comparison of beer-Lambert's law and light transport equation. *Engineered Science*, *24*(2), Article 912. https://doi.org/10.30919/es912

Sajjadi, A. Y., Mitra, K., & Guo, Z. (2013). Thermal analysis and experiments of laser− tissue interactions: A review. *Heat Transfer Research*, *44*(3-4), 345-388. https://doi.org/10.1615/HeatTransRes.2012006425

Seidabadi, L., Vandenbussche, I., Carter Fink, R., Moore, M., McCorkendale, B., & Esmailie, F. (2025). Role of computational modelling in enhancing thermal safety during cardiac ablation. *Interdisciplinary CardioVascular and Thoracic Surgery*, *40*(8), Article ivaf184. https://doi.org/10.1093/icvts/ivaf184

Singh, S., & Melnik, R. (2020). Thermal ablation of biological tissues in disease treatment: A review of computational models and future directions. *Electromagnetic Biology and Medicine*, *39*(2), 49-88. https://doi.org/10.1080/15368378.2020.1741383

Suzuki, W., Ietani, K., Makabe, T., Oki, S., Ohno, A., Mikami, Y., & Yamashita, H. (2024). Prognostic outcome of cervical laser ablation using a holmium yttrium-aluminum-garnet (Ho: YAG) laser for the treatment of cervical intraepithelial neoplasia: A single-center retrospective study. *Gynecologic Oncology Reports*, *53*, Article 101405. https://doi.org/10.1016/j.gore.2024.101405

Waghe, T., Acharya, N., & Waghe Jr, T. (2024). Advancements in the management of cervical intraepithelial neoplasia: A comprehensive review. *Cureus*, *16*(4), Article e58645. https://doi.org/10.7759/cureus.58645

Walker, D. C., Brown, B. H., Smallwood, R. H., Hose, D. R., & Jones, D. M. (2002). Modelled current distribution in cervical squamous tissue. *Physiological Measurement*, *23*(1), 159-168. https://doi.org/10.1088/0967-3334/23/1/315

Wongchadakul, P., & Rattanadecho, P. (2021). Mathematical modeling of multilayered skin with embedded tumor through combining laser ablation and nanoparticles: Effects of laser beam area, wavelength, intensity, tumor absorption coefficient and its position. *International Journal of Heat and Technology*, *39*(1), 89–100. https://doi.org/10.18280/ijht.390109

World Health Organization. (2019). *WHO guidelines for the use of thermal ablation for cervical pre-cancer lesions*. World Health Organization. Retrieved from https://apps.who.int/iris/bitstream/handle/10665/329299/9789241550598-eng.pdf

Xiao, L., Guo, J., Wang, H., He, Q., Xu, Y., Yuan, L., ... & Chen, H. (2023). Thermal damage and the prognostic evaluation of laser ablation of bone tissue a review. *Lasers in Medical Science*, *38*(1), Article 205. https://doi.org/10.1007/s10103-023-03868-1

Xu, M., Xu, D., Deng, Z., Tian, G., & Jiang, T. A. (2023). Long-term outcomes of endoscopic ultrasound-guided laser ablation for liver tumors in the caudate lobe: 5 years of experience. *Scandinavian Journal of Gastroenterology*, *58*(5), 558-564. https://doi.org/10.1080/00365521.2022.2148833